



# Nuclear clusters as the first stepping stones for the chemical evolution of the universe

Michael Wiescher<sup>1,a</sup>, Ondrea Clarkson<sup>2</sup>, Richard J. deBoer<sup>1</sup> , Pavel Denisenkov<sup>2</sup>

<sup>1</sup> Department of Physics, The Joint Institute for Nuclear Astrophysics, University of Notre Dame, Notre Dame, Indiana 46556, USA

<sup>2</sup> Department of Physics & Astronomy, University of Victoria, Victoria, BC V8W 2Y2, Canada

Received: 23 October 2020 / Accepted: 23 December 2020 / Published online: 13 January 2021

© The Author(s), under exclusive licence to Società Italiana di Fisica and Springer-Verlag GmbH Germany, part of Springer Nature 2021

Communicated by Nicolas Alamanos

**Abstract** It is a well-established fact that the generation of the heavy elements occurred in stars—the Cauldrons of the Cosmos—via multiple complex nuclear reaction processes during stellar life and death. This paper will address the question of the first step, the formation of heavier elements such as carbon and oxygen from the primordial elemental abundance distribution in first stars. This nucleosynthesis can be facilitated by nuclear clustering of primordial isotopes in hot and highly convective first stars, provided that a helium rich or hydrogen depleted environment is available. The paper will summarize the associated nuclear reactions and the nucleosynthesis paths linking  $^4\text{He}$  to  $^{12}\text{C}$ . This will be based on an analysis of new experimental data for several of the anticipated nuclear reactions, and the role they might play at different temperature and density conditions in first star matter.

## 1 Introduction

Big Bang nucleosynthesis and the production of a primordial abundance distribution is well-established [1–3] and the comparison between the predicted and observed primordial abundances provides strong evidence for the Big Bang model. Contrary to very early suggestions [4], which proposed an instantaneous production of the observed galactic abundance distribution in the primeval fireball, we now know that the abundance distribution from Big Bang nucleosynthesis (BBN) is largely confined to light elements from hydrogen to helium and lithium. This is explained by the mass 5 and mass 8 gaps; the homogeneity of the early universe and the lack of stable or long-lived isotopes at these masses prohibits proton, neutron, or  $\alpha$ -capture reactions, which would facilitate the production of heavier nuclei in the CNO range

and beyond [5]. The so-called Li-problem, associated with fundamental differences in the predicted and observed Li isotopic abundances, is the remaining inconsistency in our interpretation of BBN [6, 7]. In terms of  $^7\text{Li}$ , the BBN predictions disagree with the measured primordial abundances, being substantially higher than the observations. Depending on the treatment of systematic uncertainties, the discrepancy is a factor  $^7\text{Li}_{BB} / ^7\text{Li}_{obs} = 2.4\text{--}4.3$ , representing a substantial discrepancy. On the other hand,  $^6\text{Li}$  observations indicate much higher values than predicted by the BBN models.

Another question is associated with the nucleosynthesis processes in a first star environment. The predicted mass distribution for these primordial stars is between 5 and  $120 M_{\odot}$  [8]. These stars formed about 400 million years after the Big Bang, and their lifetime is far smaller than the 13.6 billion year age of the universe. Primordial stars are long gone, but we can observe the reflection of their nucleosynthesis contributions in the strong carbon, nitrogen, and oxygen pattern of long-lived second or third generation stars [9]. Massive primordial stars have a fundamental problem in that, unlike younger stars, they cannot stabilize on the main sequence through the CNO cycles. Instead, their energy generation, in the hydrogen-burning phase, relies entirely on the  $pp$ -chains [10]. The energy production rate is limited by the available fuel and by the weak interaction based  $p+p$  fusion process [11]. The star therefore cannot stabilize and is expected to have core contraction until high enough temperature and density conditions are reached that the  $3\alpha$  and subsequent  $^{12}\text{C}(\alpha, \gamma)^{16}\text{O}$  process are triggered.

The traditional view was, therefore, that during the core contraction, the density and temperature conditions would gradually increase. Eventually the ignition of the  $3\alpha$ -process occurs, generating carbon and oxygen, which may then facilitate a CNO process on the remaining hydrogen fuel. The evolution of such stars have been recently explored in a grid of 26 stellar models between 15 and  $140 M_{\odot}$  to explore a

<sup>a</sup>e-mail: [Michael.C.Wiescher.1@nd.edu](mailto:Michael.C.Wiescher.1@nd.edu) (corresponding author)

number of assumptions on convection and mixing conditions. Temperatures ranging from  $9 \times 10^7$  to  $1.6 \times 10^8$  K and densities conditions from 10 to  $250 \text{ g/cm}^3$  were investigated [12]. The corresponding Gamow energy range (see, e.g., [13]) for the reactions considered here is below 200 keV center-of-mass energy, an energy range which has not been reached by experiment. Evaluating the reaction rates therefore requires a full understanding of the reaction contributions towards the Gamow range, since an extrapolation from higher energy data must be performed.

The  $3\alpha$ -process is certainly one of the key examples of the impact of nuclear clusters on stellar burning processes [14, 15]. It is a two-step process, in which the first step of  ${}^4\text{He}+{}^4\text{He}$  produces a very short-lived  ${}^8\text{Be}$ . The equilibrium abundance of this configuration allows a third  $\alpha$ -capture process, through a three  $\alpha$ -cluster configuration in the  ${}^{12}\text{C}$  compound nucleus, the Hoyle state [16–18]. The  $\alpha$ -cluster configuration of the compound nuclei involved, such as  ${}^8\text{Be}$ ,  ${}^{12}\text{C}$ , and  ${}^{16}\text{O}$ , is well established and is responsible for facilitating helium burning through the  $\alpha$ -process in Red Giant Stars. The cluster structure of the associated nuclei has been studied in great detail and is responsible for the fine-tuning of this fundamental reaction sequence [19].

While the impact of cluster states on the  $\alpha$ -process is well studied and documented, there are a number of other possible reaction sequences that may facilitate a reaction flow. Here the focus is on the primordial abundance distribution to the CNO range through near threshold  $\alpha$ -cluster configurations in light nuclei [20]. These reaction sequences may not only provide a transport path towards higher masses at lower temperature and density conditions as required by the  $\alpha$ -process, but may also impact the  ${}^6\text{Li}$  and  ${}^7\text{Li}$  abundances and therefore the lithium problem [21].

The  $\alpha$ -cluster structure of  ${}^6\text{Li}$  [22],  ${}^{10}\text{B}$  [23], and  ${}^{14}\text{N}$  [24, 24], is characterized by a  $d \otimes \alpha$  configuration and the parallel isotope sequence  ${}^7\text{Li}$ ,  ${}^{11}\text{B}$  [25],  ${}^{15}\text{N}$ ,  ${}^{19}\text{F}$  by  $t \otimes \alpha$  configurations. Such configurations are all responsible for the emergence of strong  $\alpha$ -cluster resonances near the  $\alpha$ -threshold in the respective compound nuclei. In these cases, only in the  ${}^{14}\text{N}$  and  ${}^{15}\text{N}$  compound systems are the neutron channels open, making  ${}^{10}\text{B}$  and  ${}^{11}\text{B}(\alpha, n)$  strong neutron sources. In the other cases the neutron channel is closed at low energies and the  $\gamma$ -channel dominates, such as in the  ${}^6\text{Li}$  and  ${}^7\text{Li}(\alpha, \gamma)$  reactions.

Such  $\alpha$ -induced reactions feed on the interaction between  ${}^4\text{He}$  and other primordial light isotopes forming near-threshold cluster configurations of the type  $d \otimes (n \times \alpha)$  (with  $n = 1, 2, 3, \dots$ ) such as  ${}^6\text{Li}$ ,  ${}^{10}\text{B}$  and  ${}^{14}\text{N}$  as well as  $t \otimes (n \times \alpha)$  (with  $n = 1, 2, 3, \dots$ ) such as  ${}^7\text{Li}$ ,  ${}^{11}\text{B}$  and  ${}^{15}\text{N}$  along the line of stability. This might cause the emergence of reaction sequences such as  ${}^2\text{H}(\alpha, \gamma){}^6\text{Li}(\alpha, \gamma){}^{10}\text{B}$  followed by  ${}^{10}\text{B}(\alpha, n)$ ,  ${}^{10}\text{B}(\alpha, p)$  and  ${}^{10}\text{B}(\alpha, \gamma)$ , forming  ${}^{13}\text{N}$ ,  ${}^{13}\text{C}$ , and  ${}^{14}\text{N}$ , respectively, depending on the

strengths of the various reaction channels. Similarly a second reaction link may emerge, fed by the initial  ${}^3\text{He}$  abundance,  ${}^3\text{He}(\alpha, \gamma){}^7\text{Be}(e^- \nu){}^7\text{Li}(\alpha, \gamma){}^{11}\text{B}$ , with subsequent  ${}^{11}\text{B}(\alpha, n){}^{14}\text{N}$ ,  ${}^{11}\text{B}(\alpha, p){}^{14}\text{C}$ , and  ${}^{11}\text{B}(\alpha, \gamma){}^{15}\text{N}$  reactions. Both reaction sequences will feed the CNO mass range in a helium enriched primordial star environment.

However, pronounced  $\alpha$ -cluster mirror configurations such as  ${}^3\text{He} \otimes (n \times \alpha)$  (with  $n = 1, 2, 3, \dots$ ) such as  ${}^{7,8}\text{Be}$ , and  ${}^{11,12}\text{C}$  can be formed by proton capture causing strong reprocessing by  $\alpha$ -emission via  ${}^6,7\text{Li}(p, \alpha){}^{3,4}\text{He}$  and  ${}^{10,11}\text{B}(p, \alpha){}^{7,8}\text{Be}$  reactions. This prohibits a strong reaction link between the  $pp$ -chains and the CNO cycles in stellar hydrogen burning. Therefore, the proposed  $\alpha$ -induced reaction paths will only be feasible in largely hydrogen depleted primordial stellar matter, where the mass fraction of hydrogen is  $X \leq 10^{-6}$ . Such conditions may emerge due to deep convective processes in early star environments, e.g., during hydrogen ingestion into a helium convective zone.

In this paper, we provide an overview of the observation and analysis of such  $\alpha$ -cluster states near the threshold for some of the  $\alpha$ -capture reactions mentioned above. We performed a number of  $\alpha$ -induced reaction studies on Li and B isotopes to identify direct or indirect signatures of such resonance states towards low energies and found very pronounced  $\alpha$ -clustering close to the thresholds. These near-threshold  $\alpha$ -cluster resonances enhance the associated rates by many orders of magnitude. We have performed detailed  $R$ -matrix analysis of the new and previous data sets on capture, transfer, and scattering data to determine the impact on the reaction rates. We also performed an impact study on the nucleosynthesis pattern in primordial environments to investigate the affect of these reaction sequences for different levels of hydrogen in primordial abundance distributions.

## 2 Nuclear data

To explore the nature of the  $\alpha$ -cluster structure near the  $\alpha$ -threshold of light nuclei, along the here proposed reaction chain, either  $\alpha$ -transfer or more directly low energy  $\alpha$ -capture reactions can be used. We primarily focused on low energy  $\alpha$ -capture measurements for this study, but also take into account the information from corresponding transfer measurements. The number of  $\alpha$ -capture measurements on stable lithium and boron isotopes is limited. The existing measurements have mostly focused on higher energies, well above the  $\alpha$ -threshold in the respective compound nuclei. We have developed an experimental program to extend the existing data towards lower energies.

The  ${}^6\text{Li}(\alpha, \gamma){}^{10}\text{B}$  reaction has a  $Q$ -value of 4.461 MeV [26, 27].  ${}^6\text{Li}({}^6\text{Li}, d){}^{10}\text{B}$  transfer reactions indicate a pronounced  $3^+$  state at  $E_x = 4.761$  MeV corresponding to a

resonance at 300 keV center-of-mass energy in the  $\alpha$ -capture reaction channel [28]. This state has indeed been observed as a resonance in the  ${}^6\text{Li}(\alpha, \gamma){}^{10}\text{B}$  reaction with several higher energy cluster resonances [29]. New measurements are in the planning stage, but the present analysis will rely solely on literature data.

The  ${}^7\text{Li}(\alpha, \gamma){}^{11}\text{B}$  reaction has a  $Q$ -value of 8.664 MeV [26, 27]. At low energies, the cross section is dominated by strong  $\alpha$ -cluster states that result in narrow resonances at  $E_\alpha = 401, 814, \text{ and } 953$  keV [30]. At higher energies, broad, overlapping resonances take over [31]. The energy range between 0.6 and 1.0 MeV has been explored using high resolution Ge-detectors to explore the onset of the broad state at 1.6 MeV center-of-mass energy. These results have not been published and a new study has been performed at the CASPAR underground laboratory to explore the data in more detail. This new study used the HECTOR summing detector array [32], however these results are not yet included in this analysis.

Recently the Notre Dame group has performed an extensive study on the  ${}^{10}\text{B}(\alpha, n){}^{13}\text{N}$  reaction [33]. The data suggest several resonances at center-of-mass  $\alpha$ -energies below 1.2 MeV as well as the low energy tail of a broad near-threshold state as indicated in Fig. 3. These resonances may suggest  $\alpha$ -cluster configurations near the  $\alpha$ -threshold in the  ${}^{14}\text{N}$  compound nucleus. These structures were also observed in earlier studies of the  ${}^{14}\text{N}$  compound systems through the  ${}^{10}\text{B}(\alpha, p){}^{13}\text{C}$  and the  ${}^{10}\text{B}(\alpha, d){}^{12}\text{C}$  reactions by [34, 35]. These early measurements have been confirmed by extensive low energy studies, which will be published separately [36]. The cluster nature of these states seem to be confirmed by  $\alpha$ -transfer measurements populating states in the range above the  $\alpha$  threshold [37, 38].

A similar case is the  ${}^{11}\text{B}(\alpha, n){}^{14}\text{N}$  reaction [39], where the excitation curve is characterized by broad resonance structures, which dominate the reaction rate. The cluster nature of these states seem to be confirmed by  $\alpha$ -transfer measurements populating states in the range above the  $\alpha$ -threshold [40]. These data have been complemented by recent studies at the Nuclear Science Laboratory at Notre Dame and the CASPAR accelerator [41] and inform the present analysis.

The measurements at the Nuclear Science Laboratory were made at  $E_\alpha = 520$  to 2000 keV with beam intensities on target between 0.03 and 18  $\mu\text{A}$ . A  ${}^{11}\text{B}$  enriched (99.9%) target with a thickness of  $\approx 10 \mu\text{g}/\text{cm}^2$  was created by electron sputtering enriched  ${}^{11}\text{B}$  powder onto a clean tantalum backing 0.5 mm in thickness. The detection system consisted of a  ${}^3\text{He}$  proportional counter, which was made up of 20  ${}^3\text{He}$  tubes encased in a polyethylene moderator. The detector has been described previously in Refs. [42, 43].

### 3 R-Matrix analysis and cluster structure

As all of the low  $Z$  reactions under consideration have broad resonance contributions, the phenomenological  $R$ -matrix [44] code AZURE2 [45, 46] is used to fit the experimental data and then facilitate the calculation of the reaction rate. The alternative  $R$ -matrix parameterization of Brune [47] was used to more easily connect observable energies and widths with the  $R$ -matrix calculations.

One measure of the cluster structure of a state is the dimensionless reduced  $\alpha$ -width (see, e.g., [48])

$$\theta_\alpha^2 = \gamma_\alpha^2 / \gamma_W^2, \quad (1)$$

where  $\gamma_\alpha^2$  is the observable reduced  $\alpha$ -width and  $\gamma_W^2$  is the Wigner limit

$$\gamma_W^2 = 3\hbar^2 / 2\mu a^2. \quad (2)$$

Here  $\mu$  is the reduced mass and  $a$  is the channel radius. A pure  $\alpha$ -cluster state corresponds to  $\theta_\alpha^2 \approx 1$ . Table 1 summarizes some of the properties of the near threshold levels that correspond to strong resonances observed in the reactions of interest.

Table 1 contains a few cases where  $\theta^2$  is somewhat larger than one, although in all cases it is smaller than two. There are several explanations for this discrepancy. On the experimental side, an incorrect  $J^\pi$  assignment and overestimated width determinations (or a doublet) are possible. On the theory side, it should be noted that the Wigner limit is an approximation [49] and different definitions have been used in the literature (see, e.g., [50]). Therefore somewhat larger values than one may be physical.

In this section,  $R$ -matrix analyses are presented for four different systems. It should be noted that each of these analyses is quite different in terms of the availability of experimental data and overall maturity of the  $R$ -matrix fit. For the first reaction,  ${}^6\text{Li}(\alpha, \gamma){}^{10}\text{B}$ , there are no cross section data in the literature and the calculations are made using partial widths obtained from scattering and resonance strength measurements. Therefore, these are only rough calculations and large uncertainties are present. For the  ${}^7\text{Li}(\alpha, \gamma){}^{11}\text{B}$  reaction, there are several measurements of the  ${}^7\text{Li}(\alpha, \alpha'){}^7\text{Li}$  reaction, but data for elastic scattering and capture are sparse. Further, the underlying level structure over the region of the data is rather uncertain, as there seem to be several very broad underlying states present. The fit presented is certainly not unique. For the  ${}^{10}\text{B} + \alpha$  reactions, this fit is on firmer ground, the data are described quite well by the levels reported in this region over all channels, but at lower energies, there remains considerable uncertainty regarding the level structure. Finally, for the  ${}^{11}\text{B}(\alpha, n){}^{14}\text{N}$  reaction, there are many levels over the energy range of interest. A successful multichannel fit is close to completion, but there still are some inconsistencies that may be the result of incorrect spin-parity assignments

**Table 1** Dimensionless reduced  $\alpha$ -width amplitudes for states close to the  $\alpha$ -particle threshold in  ${}^6,{}^7\text{Li}+\alpha$  and  ${}^{10,11}\text{B}+\alpha$  induced reactions

Reactants	$a$ (fm)	$J^\pi$	$E_x$ (MeV)	$\Gamma_\alpha$ (keV)	$\theta^2$		
${}^6\text{Li}+\alpha$	5.5	$3^+$	4.761	$7.8 \times 10^{-3}$	0.46		
		$2^-$	5.112	0.978	0.029		
		$2^+$	5.166	$2.9 \times 10^{-4}$	$3.5 \times 10^{-5}$		
		$1^+$	5.187	110	1.7		
		$2^+$	5.922	5.8	0.025		
		$4^+$	6.024	0.052	$8.5 \times 10^{-3}$		
		$3^-$	6.130	1.52	0.020		
		$1^-$	6.873	67	0.097		
		$2^-$	7.479	74	0.037		
		${}^7\text{Li}+\alpha$	8	$5/2^-$	8.9205	$5.6 \times 10^{-6}$	$4.7 \times 10^{-4}$
$7/2^+$	9.1835			$1.5 \times 10^{-4}$	$4.4 \times 10^{-4}$		
$5/2^+$	9.2717			4.9	0.19		
$3/2^+$	9.8612			81	0.38		
$3/2^-$	10.227			7.4	0.024		
$7/2^+$	10.3295			200	1.8		
$5/2^-$	10.3932			24	0.17		
$7/2^+$	10.6083			31	0.26		
${}^{10}\text{B}+\alpha$	5			$2^-$	12.0	$4.5 \times 10^{-5}$	0.065
				$4^-$	12.4188	0.37	0.45
		$1^+$	12.4952	0.10	0.30		
		$3^+$	12.5982	0.52	0.040		
		$3^-$	12.6890	7.3	0.90		
${}^{11}\text{B}+\alpha$	5.5	$7/2^+$	11.2389	$1.7 \times 10^{-10}$	0.041		
		$1/2^-$	11.2926	$6.1 \times 10^{-8}$	0.035		
		$1/2^+$	11.4223	$1.0 \times 10^{-4}$	0.061		
		$7/2^-$	11.4290	$1.1 \times 10^{-4}$	0.32		
		$1/2^+$	11.6186	$3.7 \times 10^{-5}$	$3.2 \times 10^{-4}$		

and insufficiencies in the modeling of the target effects. All of the analyses presented are preliminary, and are the subject of ongoing research.

### 3.1 ${}^6\text{Li}(\alpha, \gamma){}^{10}\text{B}$

For the  ${}^6\text{Li}(\alpha, \gamma)$  reaction, the lack of new cross section data means that only calculations could be made based on the level parameters available in the literature [29, 51–59] as compiled in [60]. The capture reaction has been reported to decay primarily to the ground state and first two excited states in  ${}^{10}\text{B}$ . Little is known regarding the strength of the direct capture. Upper limit estimates are made by taking a dimensionless  $\alpha$ -particle reduced width amplitude of 1 for the ground state and first excited states. New experiments have been initiated at the CASPAR underground accelerator at SURF in South Dakota and at the University of Notre Dame Nuclear Science Laboratory, but the analysis is not yet completed and will be

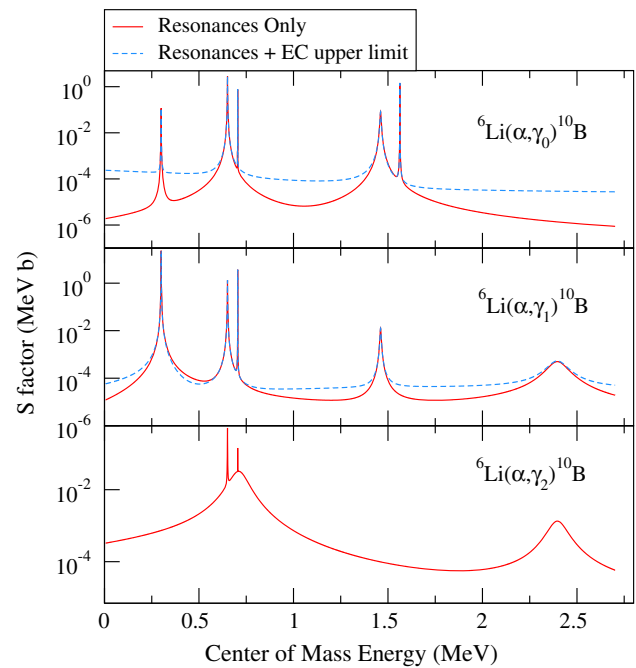


**Fig. 1** Estimate of the  ${}^6\text{Li}(\alpha, \gamma){}^{10}\text{B}$   $S$ -factor based on level parameters from the compilation [60] (red solid line). An estimate that includes an upper limit for the direct capture is also shown (blue dashed line)

presented in a later paper. Estimated  $S$ -factors are shown in Fig. 1.

### 3.2 ${}^7\text{Li}(\alpha, \gamma){}^{11}\text{B}$

The situation is somewhat better for the  ${}^7\text{Li}(\alpha, \gamma){}^{11}\text{B}$  reaction, but there are still only a few measurements. The majority of these come from [31], who measured the ground state transition over an energy range  $E_\alpha = 1.3$  to 3.2 MeV at  $\theta_\gamma = 90^\circ$ . The cross section over this region presents one large peak, but the interpretation is that it is actually the sum of several broad unresolved resonances. To give more constraint on the level contributions, the capture data was fit simultaneously with the inelastic scattering data [31, 61–65] and the scattering data [61, 64–66]. Information on the strength of narrow lower energy resonances is obtained from studies by [30]. Example data from the fit are shown in Fig. 2.

### 3.3 ${}^{10}\text{B}(\alpha, n){}^{13}\text{N}$ and ${}^{10}\text{B}(\alpha, d){}^{12}\text{C}$

The  ${}^{10}\text{B}(\alpha, n){}^{13}\text{N}$  and  ${}^{10}\text{B}(\alpha, d){}^{12}\text{C}$  reactions (as well as  ${}^{10}\text{B}(\alpha, p){}^{13}\text{C}$ ) were studied at low energies by [34, 35], but have seen very few measurements since. A low energy study of the  ${}^{10}\text{B}(\alpha, p){}^{13}\text{C}$  reaction was also made by [67]. Some higher energy measurements are available that overlap with the measurements of [34, 35], which include the  ${}^{10}\text{B}(\alpha, n){}^{13}\text{N}$  measurements of [68] and the  ${}^{10}\text{B}(\alpha, p){}^{13}\text{C}$  measurements of [69]. Low energy  $\alpha$ -scattering data is also

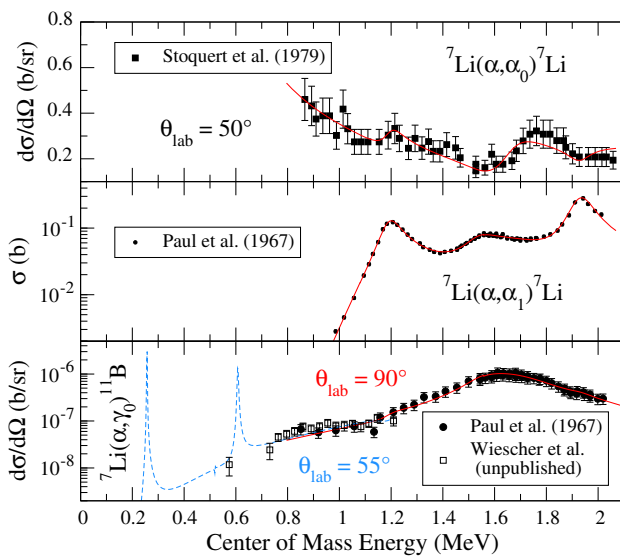


**Fig. 2** Comparison of sample data sets from [31,66] and unpublished  ${}^7\text{Li}(\alpha, \gamma_0){}^{11}\text{B}$  data with the simultaneous  $R$ -matrix fit of the elastic, inelastic, and capture data

available [70], but are limited to just a single backward angle. A recent study [33] has extended the  ${}^{10}\text{B}(\alpha, n){}^{13}\text{N}$  cross section measurements down to  $E_{c.m.} = 0.4$  MeV, were mostly limited to  $\theta_{lab} = 0^\circ$  by detector threshold and kinematics constraints. [33] observes a new upward trend in the low energy  $S$ -factor, suggesting the presence of additional low energy resonance structure (see Fig. 3). Further, the level structure seems to be well characterized, at least for levels with large  $\alpha$ -particle reduced widths, over this excitation energy range. Fig. 4 shows the enhancement of the low temperature reaction rate over that of [71], where a constant  $S$ -factor was assumed. The lower uncertainty band has been updated from that of [33], as additional measurements of the low energy  ${}^{10}\text{B}+\alpha$  reactions, that are currently underway at the University of Notre Dame, have confirmed the presence of additional lower energy resonances.

### 3.4 ${}^{11}\text{B}(\alpha, n){}^{14}\text{N}$

The only low energy, high precision  ${}^{11}\text{B}(\alpha, n){}^{14}\text{N}$  cross section study is that of [39]. In that work, measurements of the  ${}^{11}\text{B}(\alpha, p){}^{14}\text{C}$  and  ${}^{14}\text{C}(p, n){}^{14}\text{N}$  reactions were also made over a similar excitation energy range in the  ${}^{15}\text{N}$  system. The level structure in this region is fairly well studied due to several measurements available for the  ${}^{14}\text{N}(n, total)$  [72, 73],  ${}^{14}\text{N}(n, p){}^{14}\text{C}$  [74–77],  ${}^{14}\text{N}(n, \alpha){}^{11}\text{B}$  [74, 76, 77],  ${}^{14}\text{C}(p, n){}^{14}\text{N}$  [75, 78–81],  ${}^{14}\text{C}(p, p){}^{14}\text{C}$  [82, 83], and  ${}^{11}\text{B}(\alpha, p){}^{14}\text{C}$  [84, 85] reactions. From these measurements, many of the levels in this region have firm  $J^\pi$  assignments, however the evaluation by [73] has found some discrepancies. Fig. 5 shows a  $R$ -matrix fit made to the new

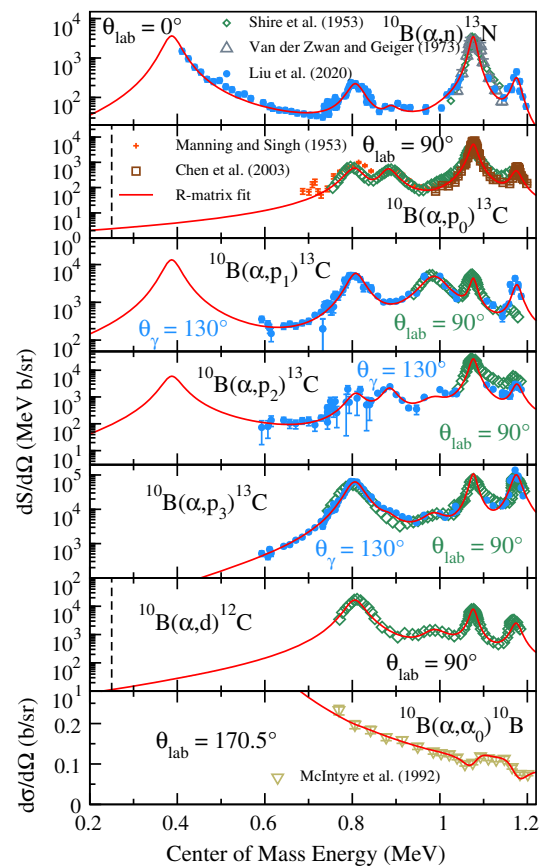


**Fig. 3** Comparison of the present  ${}^{10}\text{B}+\alpha$  measurements (blue circles) with those made previously by ([34] (green diamonds), [67] (orange crosses), [68] (grey upward triangles), [69] (brown squares), and [70] (khaki downward triangles)) at low energy. The solid red line shows the  $R$ -matrix fit from [33]. The vertical black dashed lines indicate the lower energy limits of new measurements at the University of Notre Dame [36]

data as well as to previous data across several channels. A quality fit that also includes all available angular distribution data is still underway.

## 4 Reaction rate analysis

The reaction rate for the radiative  $\alpha$ -capture on  ${}^6\text{Li}$  and  ${}^7\text{Li}$ , as well as for the total  $\alpha$ -capture on  ${}^{10}\text{B}$  and  ${}^{11}\text{B}$  feeding different exit channels into the CNO range, have been calculated by integrating the predicted  $R$ -matrix cross sections over the stellar Maxwell-Boltzmann energy distribution for temperatures in the range of 0.1–10.0 GK. The reaction rate is given by

$$N_A \langle \sigma v \rangle = \left( \frac{8}{\pi \mu} \right)^{1/2} \frac{N_A}{(k_B T)^{3/2}} \int_0^\infty \sigma(E) E e^{-E/k_B T} dE, \tag{3}$$

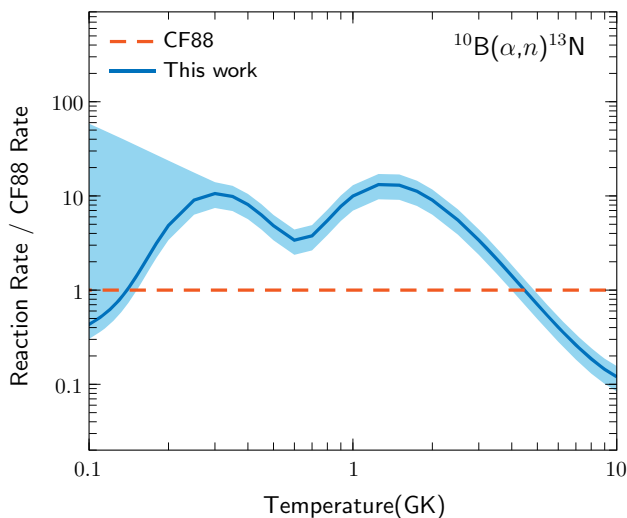


**Fig. 4** Comparison of the  $^{10}\text{B}(\alpha, n)^{13}\text{N}$  reaction rate to that of CF88 [71]. The solid blue line represents the ratio of the rate from the present work to that of CF88, while the light blue region represents the uncertainty range as described in the text. The red dashed line represents the ratio of CF88 to itself for reference. The lower limit has been revised from that of [33], based on new measurements

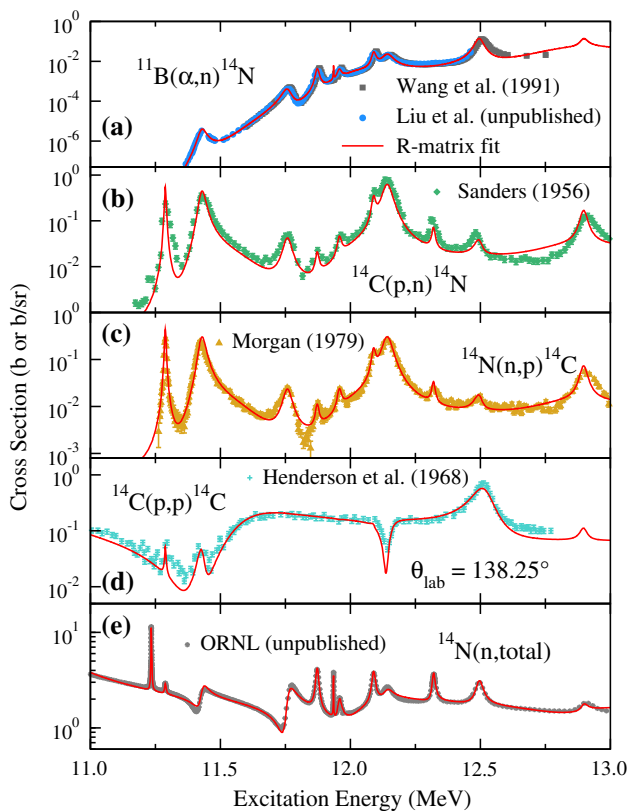


**Fig. 5** Example excitation functions from the global  $R$ -matrix fit of the  $^{15}\text{N}$  system for the present  $^{11}\text{B}(\alpha, n)^{14}\text{N}$  measurement (blue circles) and previous measurements of the  $^{11}\text{B}(\alpha, n)^{14}\text{N}$  (Ref. [39], gray squares)  $^{14}\text{C}(p, n)^{14}\text{N}$  (Ref. [81], green diamonds),  $^{14}\text{N}(n, p)^{14}\text{C}$  (Ref. [77], gold upward triangles),  $^{14}\text{C}(p, p)^{14}\text{C}$  (Ref. [83], turquoise plus), and  $^{14}\text{N}(n, \text{total})$  ([72, 73]) reactions

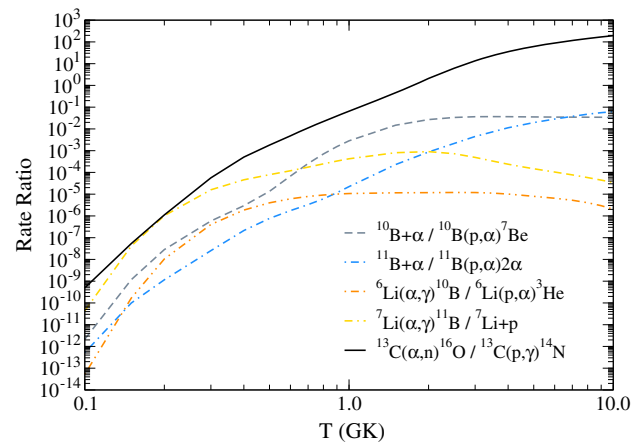


**Fig. 6** The ratios of the reaction rates for  $\alpha$ -induced and proton induced reactions on  $^{6,7}\text{Li}$ ,  $^{10,11}\text{B}$ , and  $^{13}\text{C}$  isotopes

where  $\mu$  is the reduced mass,  $E = \mu v^2/2$  is the center-of-mass energy,  $N_A$  is Avogadro's number, and  $k_B$  is Boltzmann's constant.

The new experimental data and the use of multichannel  $R$ -matrix analysis has reduced the uncertainty in the reaction rates. A significant change in the reaction rates compared to previous analysis occurs for the  $\alpha$ -induced reactions on  $^{10}\text{B}$  feeding the CNO nuclei. The newly observed broad state near the  $\alpha$ -threshold in  $^{14}\text{N}$  causes a substantial enhancement of the reaction rate at stellar temperatures, making a reaction sequence  $^2\text{H}(\alpha, \gamma)^6\text{Li}(\alpha, \gamma)^{10}\text{B}(\alpha, npd)$  feeding  $^{13}\text{N}$ ,  $^{13}\text{C}$ , and  $^{12}\text{C}$  at comparable levels possible. A reaction branch however, only becomes efficient with sufficient amount of fuel ( $^2\text{H}$ ,  $^4\text{He}$ ) and seed material (Li, B). Primordial matter is highly abundant in hydrogen and helium fuel, therefore proton induced reactions on the lithium and boron isotopes also need to be considered. While the  $\alpha$ -induced reactions are facilitated by the pronounced  $\alpha$ -cluster structure in the associated nuclei, the same is the case for the competing proton induced reactions such as  $^6\text{Li}(p, \alpha)$ ,  $^7\text{Li}(p, \alpha)$ ,  $^{10}\text{B}(p, \alpha)$ , and  $^{11}\text{B}(p, \alpha)$ , through the pronounced cluster configuration in the respective  $^7\text{Be}$ ,  $^8\text{Be}$ ,  $^{11}\text{C}$ , and  $^{12}\text{C}$  compound nuclei. With sufficient hydrogen abundance in the primordial stellar environment, these reactions open a strong back-processing reaction branch, preventing an efficient transfer of light nuclei into the CNO range. This is a similar case as for the  $^{13}\text{C}(\alpha, n)^{16}\text{O}$  neutron source in AGB stars, which is only efficient in a hydrogen free, carbon bubble environment, since the competing  $^{13}\text{C}(p, \gamma)^{13}\text{N}$  rate is orders of magnitude larger over the entire temperature range (see, e.g., Fig. 1 in [86]).

Figure 6 shows the ratio of the total rate for low energy  $\alpha$ -capture versus the rates for  $(p, \alpha)$  reactions of the respective lithium and boron isotopes. Also shown, for comparison, is the ratio of the  $^{13}\text{C}(\alpha, n)^{16}\text{O}$  rate and the compet-

**Table 2** Gamow energy ranges for the reactions investigated here at a temperature of  $T = 0.08$  GK

Reaction	Gamow energy range (keV)
${}^6,7\text{Li}+\alpha$	70–130
${}^{10,11}\text{B}+\alpha$	110–190

ing  ${}^{13}\text{C}(p, \gamma){}^{13}\text{N}$  rate. The figure indicates that the proton induced rates are in all cases several orders of magnitude larger than the competing  $\alpha$ -induced reactions due to the difference in Coulomb barrier at the relatively low temperatures considered here. For a typical primordial fuel ratio of hydrogen to helium of  $\approx 4$ , this means that a break-out via, e.g., the  ${}^6\text{Li}(\alpha, \gamma){}^{10}\text{B}(\alpha, n){}^{13}\text{N}$  reaction sequence is highly unlikely in the presence of hydrogen fuel. Therefore, this reaction sequence will only be viable in an environment that is helium enriched or hydrogen depleted by convective processes.

We have performed a number of simulations for a primordial hydrogen-depleted helium-burning environment to explore the possibility of bridging the mass 5 and mass 8 gap via a sequential  $\alpha$ -capture reaction chain versus the triple  $\alpha$ -process environment. The calculations were performed in a single-zone mode with  $T = 0.08$  GK and  $\rho = 200$  g/cm<sup>3</sup> for a hydrogen depleted, with mass fraction of  $X(\text{H}) \leq 10^{-6}$ , population III stellar evolution model. We use the NuGrid collaboration's PPN code [87] with charged-particle reactions from the JINA reaclib V1.1 [88] data base, unless the rate is replaced by the revised ones presented here. Table 2 lists the relevant Gamow energy ranges.

Figure 7 shows the reaction flux integrated over a short period of  $10^{-4}$  years, transforming the initial  ${}^3\text{He}$  by  $\alpha$ -capture into  ${}^7\text{Be}$ . Despite the low hydrogen abundance, most of the primordial  ${}^6,7\text{Li}$  is converted by  $(p, \alpha)$  reactions back to  ${}^4\text{He}$ , with the protons being produced by the  ${}^3\text{He}({}^3\text{He}, 2p){}^4\text{He}$  reaction. However the  ${}^6\text{Li}(\alpha, \gamma){}^{10}\text{B}$  and  ${}^7\text{Li}(\alpha, \gamma){}^{11}\text{B}$  reactions show already a weak branch towards boron isotopes within the short burning period. The  ${}^6\text{Li}(\alpha, \gamma){}^{10}\text{B}$  flux however is particularly weak, due to the initially low  ${}^6\text{Li}$  abundance. The elemental abundances are still confined to the region below the  $A = 8$  mass gap.

The alternative branch,  ${}^7\text{Li}(\alpha, \gamma){}^{11}\text{B}$ , is substantially stronger since it is continuously fed via the  ${}^3\text{He}(\alpha, \gamma){}^7\text{Be}(e^-){}^7\text{Li}$  reaction. Calculations over longer burning periods clearly demonstrate the emergence of the reaction chain  ${}^3\text{He}(\alpha, \gamma){}^7\text{Be}(e^-){}^7\text{Li}(\alpha, \gamma){}^{11}\text{B}(\alpha, n){}^{14}\text{N}$  with a weaker  ${}^{11}\text{B}(\alpha, p){}^{14}\text{C}$  branch (Fig. 8). At these temperatures a second reaction branch towards  ${}^{11}\text{B}$  emerges via the direct  $\alpha$ -capture reaction  ${}^7\text{Be}(\alpha, \gamma){}^{11}\text{C}(\beta^+ \nu){}^{11}\text{B}$ .  ${}^7\text{Li}$  is the critical stepping stone and this reaction links to the CNO range, feeding entirely on the initial abundance of  ${}^3\text{He}$ . After about 10 years, the  $3\alpha$  process begins to emerge, gradually com-

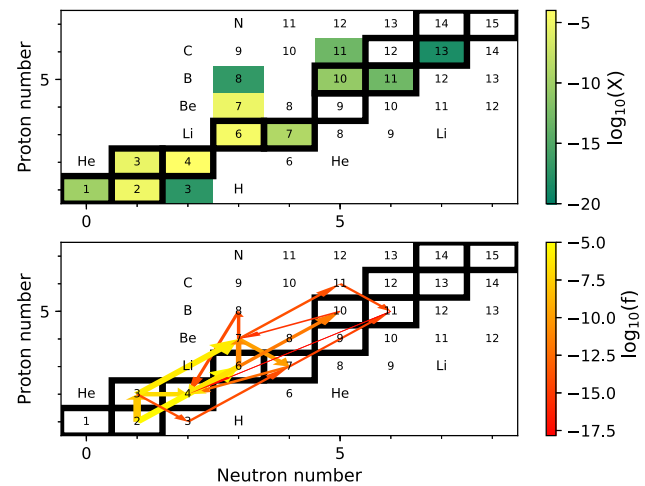


**Fig. 7** The abundance distribution (top panel, where  $X$  is the mass fraction) and reaction flux (bottom panel, where  $f = \int_0^t (\delta Y_i / \delta t)_j dt$ , shows a time-integrated variation rate of the abundance  $Y_i = X_i/A_i$  due to the reaction  $j$ ) at the onset of helium burning ( $t = 10^{-4}$  y) in a hydrogen depleted,  $X(\text{H}) \leq 10^{-6}$ , primordial environment.  ${}^3\text{He}$  is converted to  ${}^7\text{Be}$  and small fractions of  ${}^6\text{Li}$  and  ${}^7\text{Li}$  are processed to  ${}^{10}\text{B}$  and  ${}^{11}\text{B}$  respectively. However a fair amount is processed back by  ${}^6,7\text{Li}(p, \alpha){}^3,4\text{He}$  fueled by the  ${}^3\text{He}({}^3\text{He}, 2p)$  reactions

peting in the transfer from light nuclei into the CNO mass range (Fig. 9).

Figures 7, 8 and 9 show the reaction fluxes at different time steps  $t = 10^{-4}$ , 0.8, and 10 years after the onset of the simulations to represent the dynamics of the nucleosynthesis development. After  $t = 10^{-4}$  y, or about one hour, the flux and abundance diagram show that the  $A = 8$  mass gap has been bridged by several reactions with  ${}^6,7\text{Li}(\alpha, \gamma){}^{10,11}\text{B}$  and  ${}^7\text{Be}(\alpha, \gamma){}^{11}\text{C}(\beta^+ \nu){}^{11}\text{B}$  providing the strongest links across the gap. The flow via the  $3\alpha$ -process appears orders of magnitude weaker. At this time, most of the  ${}^{11}\text{B}$  is processed back via the  ${}^{11}\text{B}(p, 2\alpha){}^4\text{He}$  reaction with only a weak  ${}^{11}\text{B}(p, \gamma)$  branch starting to feed  ${}^{12}\text{C}$ . At  $t = 0.8$  years, or 10 months, with the abundances of  ${}^6,7\text{Li}$  and  ${}^6,7\text{Be}$  near their maximum, this process has solidified. Back-processing from the boron range is reduced due to the decline in hydrogen abundance and the  ${}^{11}\text{B}$  is distributed increasingly via the  ${}^{11}\text{B}(\alpha, n){}^{14}\text{N}$  branch into the CNO range. The second emerging branch, via the  ${}^6\text{Li}(\alpha, \gamma)$  reaction, feeds  ${}^{10}\text{B}$  and is gradually processed further by the  ${}^{11}\text{B}(\alpha, p){}^{13}\text{C}$  reaction and to a lesser degree by the  ${}^{11}\text{B}(\alpha, n){}^{13}\text{N}$  reaction into the CNO mass range. The  $3\alpha$ -process is still negligible. This is also the case at  $t = 10$  years, a steady flow of material fed by the transformation of the existing light primordial isotopes facilitates this flux rapidly feeding the CNO range. Even at this time, the  $3\alpha$ -process remains negligible.

Figure 10 shows the corresponding development of the isotopic abundances in the light element range being gradually converted from the primordial  ${}^2\text{H}$ ,  ${}^3\text{He}$ , and Li abundance towards the boron isotopes and eventually into the

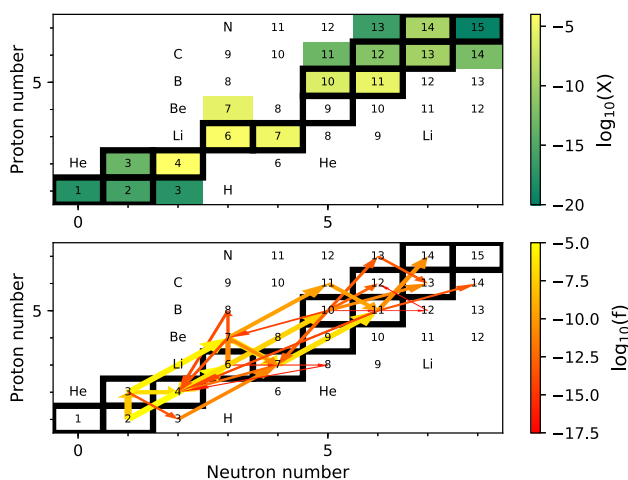


**Fig. 8** The abundance distribution and reaction flux during an early period of helium burning ( $t = 0.8$  years) in a hydrogen depleted primordial environment

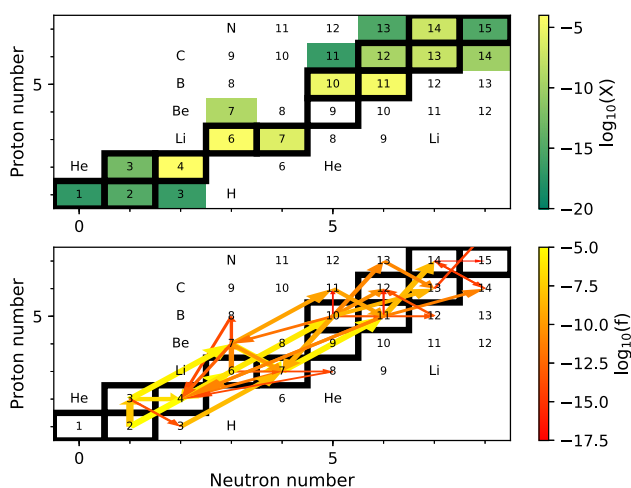


**Fig. 9** The abundance distribution and reaction flux after several years of helium burning ( $t = 10$  years) in a hydrogen depleted primordial environment

CNO range, represented by  $^{14}\text{N}$ . The dashed lines show the impact of the new reaction rates, which accelerate the nucleosynthesis processes, fed primarily by the interaction of the light primordial  $^2\text{H}$  and  $^3\text{He}$  isotopes with the primordial  $^4\text{He}$ .

This simulation is done with the assumption of no hydrogen, to demonstrate the feasibility of the process, even small amounts of hydrogen delay the nucleosynthesis towards heavier elements due to strong ( $p, \alpha$ ) back-processing as demonstrated in Fig. 6. The hydrogen-reduced scenario presented here, may only emerge as a consequence of mixing processes, as in the case of the carbon bubble in AGB stars or at the end of the hydrogen burning and the on-set of helium burning in a first generation star.

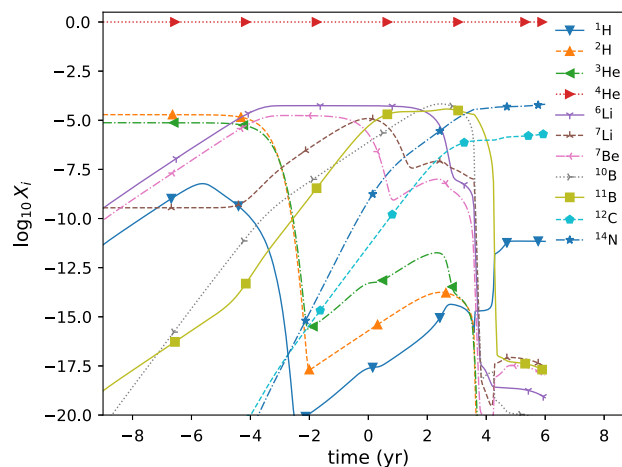


**Fig. 10** The evolution of the light element abundances of  $^1\text{H}$ ,  $^2\text{H}$ ,  $^3\text{He}$ ,  $^4\text{He}$ ,  $^6\text{Li}$ ,  $^7\text{Li}$  as primordial isotopes and  $^{10}\text{B}$ ,  $^{11}\text{B}$ ,  $^{12}\text{C}$ , and  $^{14}\text{N}$  as nucleosynthesis products, over the first million years of helium burning in an initially hydrogen depleted primordial environment ( $X(\text{H}) = 0$  at  $t = 0$ )

## 5 Summary

This paper represents new experimental evidence on the existence of near-threshold  $\alpha$ -cluster states in  $^{10}\text{B}$ ,  $^{11}\text{B}$ ,  $^{14}\text{N}$  and  $^{15}\text{N}$  isotopes, which enhance the reaction rates for  $\alpha$ -capture reactions on lithium and boron isotopes.  $R$ -matrix techniques have been utilized to make predictions for the associated reaction rates over a wide stellar temperature range. The inclusion of the cluster states causes a significant enhancement of the rates. A first order simulation of the associated nucleosynthesis process, at typical temperature and density conditions of first generation stars, has been performed to investigate the impact of these reactions. For that purpose, a primordial abundance has been used, but without hydrogen, to minimize the impact of the strong back-processing ( $p, \alpha$ ) reactions on lithium and boron isotopes. The results demonstrate that, under these circumstances, lithium and boron emerge as pronounced stepping stones in the conversion of primordial  $^2\text{H}$  and  $^3\text{He}$  into carbon and nitrogen. This triggers a fast feeding mechanism for the CNO cycle in first generation stars prior to the on-set of the  $3\alpha$ -process. In the mode presented here for static temperature and density conditions, the statements remain valid up to hydrogen mass fractions of  $10^{-6}$ . Coupled to the new experimental effort at lower energies at the US underground accelerator laboratory, CASPAR, new and more detailed simulations are being planned to investigate in detail the role of hydrogen in this process. These investigations continue to further our understanding of the impact of dynamic convection and dredge-up processes anticipated for the first star environments.

**Acknowledgements** This research utilized resources from the Notre Dame Center for Research Computing and was supported by the

National Science Foundation through Grant No. Phys-2011890, and the Joint Institute for Nuclear Astrophysics through Grant No. Phys-1430152 (JINA Center for the Evolution of the Elements).

**Data Availability Statement** This manuscript has no associated data or the data will not be deposited. [Authors' comment: The data shown here are preliminary. Data will be made available in future publications.]

## References

- Robert V. Wagoner, William A. Fowler, F. Hoyle, On the synthesis of elements at very high temperatures. *Astrophys. J.* **148**, 3 (1967)
- David N. Schramm, Primordial nucleosynthesis. *Proc. Natl. Acad. Sci.* **95**(1), 42–46 (1998)
- Richard H. Cyburt, Brian D. Fields, Keith A. Olive, Tsung-Han Yeh, Big bang nucleosynthesis: Present status. *Rev. Mod. Phys.* **88**, 015004 (Feb 2016)
- R.A. Alpher, H. Bethe, G. Gamow, The origin of chemical elements. *Phys. Rev.* **73**, 803–804 (Apr 1948)
- Thomas Rauscher, James H. Applegate, John J. Cowan, Friedrich-Karl Thielemann, Michael Wiescher, Production of heavy elements in inhomogeneous cosmologies. *Astrophys. J.* **429**, 499 (1994)
- Sean G. Ryan, Timothy C. Beers, Keith A. Olive, Brian D. Fields, John E. Norris, Primordial lithium and big bang nucleosynthesis. *Astrophys. J.* **530**(2), L57–L60 (2000)
- Richard H. Cyburt, Brian D. Fields, Keith A. Olive, An update on the big bang nucleosynthesis prediction for  ${}^7\text{Li}$ : the problem worsens. *J. Cosmol. Astroparticle Phys.* **2008**(11), 012 (2008)
- M. Fraser, A.R. Casey, G. Gilmore, A. Heger, C. Chan, The mass distribution of Population III stars. *Mon. Notices R. Astronomical Soc.* **468**(1), 418–425,02 (2017)
- S.C. Keller, M.S. Bessell, A. Frebel, A.R. Casey, M. Asplund, H.R. Jacobson, K. Lind, J.E. Norris, D. Yong, A. Heger, Z. Magic, G.S. Da Costa, B.P. Schmidt, P. Tisserand, A single low-energy, iron-poor supernova as the source of metals in the star SMSS J031300.36-670839.3. *Nature* **506**, 463–466 (2014)
- E.E. Salpeter, Nuclear Reactions in the Stars. I. Proton-Proton Chain. *Phys. Rev.* **88**, 547–553 (Nov 1952)
- M. Wiescher, J. Görres, S. Graff, L. Buchmann, F.K. Thielemann, The hot Proton-Proton chains in low-metallicity objects. *Astrophys. J.* **343**, 352 (1989)
- O Clarkson and F Herwig. Convective H-He Interactions in Massive Population III Stellar Evolution Models. *Monthly Notices of the Royal Astronomical Society*, 10 (2020). staa3328
- Christian Iliadis, *Nucle Phys Stars* (WILEY-VCH Verlag GmbH & Co. KGaA, Weinheim, 2007)
- J.-P. Ebran, T. Nikšić, E. Khan, D. Vretenar, How atomic nuclei cluster. *Nature* **487**, 341–344 (2012)
- H. Oberhummer, A. Csótó, H. Schlattl, Stellar production rates of carbon and its abundance in the universe. *Science* **289**(5476), 88–90 (2000)
- S.I. Fedotov, O.I. Kartavtsev, V.I. Kochkin, A.V. Malykh,  $3\alpha$ -cluster structure of the  $0^+$  states in  ${}^{12}\text{C}$  and the effective  $\alpha - \alpha$  interactions. *Phys. Rev. C* **70**, 014006 (2004)
- M. Chernykh, H. Feldmeier, T. Neff, P. von Neumann-Cosel, A. Richter, Structure of the Hoyle State in  ${}^{12}\text{C}$ . *Phys. Rev. Lett.* **98**, 032501 (2007)
- S.I. Fedotov, O.I. Kartavtsev, A.V. Malykh, Effective three-body interactions in the  $\alpha$ -cluster model for the  ${}^{12}\text{C}$  nucleus. *Eur. Phys. J. A* **26**, 201–207 (2005)
- T.A. Lähde, U. Meißner, E. Epelbaum, An update on fine-tuning in the triple-alpha process. *Eur. Phys. J. A* **56**, 89 (2020)
- W. von Oertzen, Martin Freer, Yoshiko Kanada-En'yo, Nuclear clusters and nuclear molecules. *Phys. Rep.* **432**(2), 43–113 (2006)
- T. Hansen, C.J. Hansen, N. Christlieb, D. Yong, M.S. Bessell, A.E. García Pérez, T.C. Beers, V.M. Placco, A. Frebel, J.E. Norris, M. Asplund, Exploring the origin of lithium, carbon, strontium, and barium with four new ultra metal-poor stars. *Astrophys. J.* **787**(2), 162 (2014)
- Guillaume Hupin, Sofia Quaglioni, Petr Navrátil, Unified description of  ${}^6\text{Li}$  structure and deuterium- ${}^4\text{He}$  dynamics with chiral two- and three-nucleon forces. *Phys. Rev. Lett.* **114**, 212502 (2015)
- H. Nishioka, Two-alpha-particle-plus-dinucleon-cluster model for  ${}^{10}\text{B}$  and  ${}^{10}\text{Be}$ . *J. Phys. G* **10**(12), 1713–1729 (1984)
- Yoshiko Kanada-En'yo,  ${}^{10}\text{B} + \alpha$  states with chain-like structures in  ${}^{14}\text{N}$ . *Phys. Rev. C* **92**, 064326 (2015)
- T. Kawabata, H. Akimune, H. Fujita, Y. Fujita, M. Fujiwara, K. Hara, K. Hatanaka, M. Itoh, Y. Kanada-En'yo, S. Kishi, K. Nakanishi, H. Sakaguchi, Y. Shimbara, A. Tamii, S. Terashima, M. Uchida, T. Wakasa, Y. Yasuda, H.P. Yoshida, M. Yosoi,  $2\alpha + t$  cluster structure in  ${}^{11}\text{B}$ . *Phys. Lett. B* **646**(1), 6–11 (2007)
- W.J. Huang, G. Audi, F.G. Meng Wang, S.Naimi Kondev, Xu Xing, The AME2016 atomic mass evaluation (I). Evaluation of input data and adjustment procedures. *Chin. Phys. C* **41**(3), 030002 (2017)
- G. Meng Wang, F.G. Audi, W.J. Kondev, S.Naimi Huang, Xu Xing, The AME2016 atomic mass evaluation (II). Tables, graphs and references. *Chin. Phys. C* **41**(3), 030003 (2017)
- K.G. Kibler, Angular distributions and total cross sections of charged particles from  $\text{Li}^6 + \text{Li}^6$  as a function of energy. *Phys. Rev.* **152**, 932–949 (1966)
- D.E. Alburger, P.D. Parker, D.J. Bredin, D.H. Wilkinson, P.F. Donovan, A. Gallmann, R.E. Pixley, L.F. Chase, R.E. McDonald, Properties of the 4.77- and 5.16-MeV States of  $\text{B}^{10}$ . *Phys. Rev.* **143**, 692–711 (1966)
- G. Hardie, B.W. Filippone, A.J. Elwyn, M. Wiescher, R.E. Segel, Resonant alpha capture by  ${}^7\text{Be}$  and  ${}^7\text{Li}$ . *Phys. Rev. C* **29**, 1199–1206 (1984)
- P. Paul, N.G. Puttaswamy, D. Kohler, Excited States in  $\text{B}^{11}$  Observed in the  $\text{Li}^7(\alpha, \gamma)$  Reaction. *Phys. Rev.* **164**, 1332–1342 (1967)
- Hanhardt. in preparation
- Q. Liu, M. Febraro, R.J. deBoer, S. Aguilar, A. Boeltzig, Y. Chen, M. Couder, J. Görres, E. Lamere, S. Lyons, K.T. Macon, K. Manukyan, L. Morales, S. Pain, W.A. Peters, C. Seymour, G. Seymour, R. Toomey, B. Vande Kolk, J. Weaver, M. Wiescher, Low-energy cross-section measurement of the  ${}^{10}\text{B}(\alpha, n){}^{13}\text{N}$  reaction and its impact on neutron production in first-generation stars. *Phys. Rev. C* **101**, 025808 (2020)
- E.S. Shire, J.R. Wormald, G. Lindsay-Jones, A. Lundén, A.G. Stanley, Nuclear reactions produced by the bombardment of boron by low energy alpha particles. *Phil. Mag.* **44**(358), 1197–1212 (1953)
- E.S. Shire, R.D. Edge, The production of neutrons and protons by the bombardment of boron by low energy alpha-particles. *Phil. Mag.* **46**(377), 640–651 (1955)
- A. Gula, R.J. deBoer, K. Manukyan, M. Wiescher, R. Kelmar, S. Aguilar, S. Henderson, S. Moylan, J. Wilkinson, B. Frentz, S. McGuinness, C. Seymour, S. Shahina, J. Arroyo, and C. Boomer-shine. In preparation
- W. Kohler, G. Gruber, A. Steinhauser, K. Bethge, Nuclear reactions of 24 MeV  ${}^7\text{Li}$  on  ${}^{10}\text{B}$ . *Nucl. Phys. A* **290**(1), 233–252 (1977)
- M.E. Clark, K.W. Kemper, Transfer reaction studies to states in  ${}^{14}\text{N}$  and  ${}^{14}\text{C}$ . *Nucl. Phys. A* **425**(1), 185–204 (1984)
- T.R. Wang, R.B. Vogelaar, R.W. Kavanagh,  ${}^{11}\text{B} + \alpha$  reaction rates and primordial nucleosynthesis. *Phys. Rev. C* **43**, 883–896 (1991)
- W. Kohler, H. Schmidt-Böcking, K. Bethge, Investigation of  ${}^{15}\text{N}$  by the reactions  ${}^{11}\text{B}({}^7\text{Li}, t){}^{15}\text{N}$  and  ${}^{10}\text{B}({}^7\text{Li}, d){}^{15}\text{N}$ . *Nucl. Phys. A* **262**(1), 113–124 (1976)
- M. Wiescher, R.J. deBoer, J. Görres, A. Gula, Q. Liu, Neutron sources in early stars. *Acta Phys. Pol. B* **51**, 631 (2020)

42. A. Best, M. Beard, J. Görres, M. Couder, R. deBoer, S. Falahat, R.T. Güray, A. Kontos, K.-L. Kratz, P.J. LeBlanc, Q. Li, S. O'Brien, N. Özkan, M. Pignatari, K. Sonnabend, R. Talwar, W. Tan, E. Uberseder, M. Wiescher, Measurement of the reaction  $^{17}\text{O}(\alpha, n)^{20}\text{Ne}$  and its impact on the  $s$  process in massive stars. *Phys. Rev. C* **87**, 045805 (2013)
43. A. Best, S. Falahat, J. Görres, M. Couder, R. deBoer, R.T. Güray, A. Kontos, K.-L. Kratz, P.J. LeBlanc, Q. Li, S. O'Brien, N. Özkan, K. Sonnabend, R. Talwar, E. Uberseder, M. Wiescher, Measurement of the reaction  $^{18}\text{O}(\alpha, n)^{21}\text{Ne}$ . *Phys. Rev. C* **87**, 045806 (2013)
44. A.M. Lane, R.G. Thomas,  $R$ -matrix theory of nuclear reactions. *Rev. Mod. Phys.* **30**, 257–353 (1958)
45. R.E. Azuma, E. Uberseder, E.C. Simpson, C.R. Brune, H. Costantini, R.J. de Boer, J. Görres, M. Heil, P.J. LeBlanc, C. Ugalde, M. Wiescher, AZURE: An  $R$ -matrix code for nuclear astrophysics. *Phys. Rev. C* **81**(4), 045805 (2010)
46. E. Uberseder and R. J. deBoer. AZURE2 User Manual, (2015)
47. C.R. Brune, Alternative parametrization of  $R$ -matrix theory. *Phys. Rev. C* **66**, 044611 (2002)
48. Yoshiko Kanada-En'yo, Tadahihiro Suhara, Yasutaka Taniguchi, (2014) Approximation of reduced width amplitude and application to cluster decay width. *Progress Theoretical Exp Phys* **7**, 07 (2014). 073D02
49. E.P. Wigner, L. Eisenbud, Higher angular momenta and long range interaction in resonance reactions. *Phys. Rev.* **72**, 29–41 (1947)
50. R.J. deBoer, J. Görres, M. Wiescher, R.E. Azuma, A. Best, C.R. Brune, C.E. Fields, S. Jones, M. Pignatari, D. Sayre, K. Smith, F.X. Timmes, E. Uberseder, The  $^{12}\text{C}(\alpha, \gamma)^{16}\text{O}$  reaction and its implications for stellar helium burning. *Rev. Mod. Phys.* **89**, 035007 (2017)
51. J.E. Nelson, J. Napolitano, S.J. Freedman,  $E2$  strength of the lowest resonance in  $^6\text{Li}(\alpha, \gamma)$ : collective effects in the  $1p$  shell. *Phys. Rev. C* **31**, 2295–2296 (1985)
52. P. Heusi, M. Berta, V. Meyer, R.E. Pixlay,  $^6\text{Li}-\alpha$  scattering below 3 MeV. *Nucl. Phys. A* **357**(2), 381–397 (1981)
53. J. Napolitano, S.J. Freedman, The width of the 5.11 MeV state in  $^{10}\text{B}$  and isovector parity mixing. *Nucl. Phys. A* **417**(2), 289–300 (1984)
54. P.D. Forsyth, H.T. Tu, W.F. Hornyak, The  $^6\text{Li}(\alpha, \gamma)^{10}\text{B}$  reaction and the energy levels of  $^{10}\text{B}$ . *Nucl. Phys.* **82**(1), 33–48 (1966)
55. R.H. Spear, Z.E. Switkowski, D.L. Kennedy, J.C.P. Heggie, Resonance strength of the 1175 keV resonance in  $^6\text{Li}(\alpha, \gamma)^{10}\text{B}$ . *Nucl. Phys. A* **318**(1), 21–28 (1979)
56. E.L. Sprenkel, J.W. Olness, R.E. Segel, Identification of doublet states at 5.16 MeV in  $\text{B}^{10}$ . *Phys. Rev. Lett.* **7**, 174–177 (1961)
57. R.E. Segel, P.P. Singh, S.S. Hanna, M.A. Grace, Gamma rays from  $\text{B}^{10}+p$ ; decay schemes and excitation functions. *Phys. Rev.* **145**, 736–745 (1966)
58. W. Auwärter, V. Meyer, Excited states of  $^{10}\text{B}$  from the  $^6\text{Li}(\alpha, \gamma)$  and  $^9\text{Be}(p, \gamma)$  reactions. *Nucl. Phys. A* **242**(1), 129–140 (1975)
59. D. Zahnow, C. Rolfs, S. Schmidt, H.P. Trautvetter, Low-energy  $S(E)$  factor of  $^9\text{Be}(p, \alpha)^6\text{Li}$  and  $^9\text{Be}(p, d)^8\text{Be}$ . *Zeitschrift für Physik A Hadrons and Nuclei* **359**, 211–218 (1997)
60. D.R. Tilley, J.H. Kelley, J.L. Godwin, D.J. Millener, J.E. Purcell, C.G. Sheu, H.R. Weller, Energy levels of light nuclei  $A = 8, 9, 10$ . *Nucl. Phys. A* **745**(3), 155–362 (2004)
61. R.Y. Cusson, Levels in  $^{11}\text{B}$  from  $^7\text{Li}(\alpha, \alpha')^7\text{Li}$  and  $^7\text{Li}(\alpha, \alpha')^7\text{Li}^*(0.48)$ . *Nucl. Phys.* **86**(3), 481–508 (1966)
62. Hans Bichsel, T.W. Bonner, Reactions  $\text{Li}^7(\alpha, n)\text{B}^{10}$ ,  $\text{Li}^7(\alpha, \alpha')\text{Li}^{7*}$ , and  $\text{B}^{10}(n, \alpha)\text{Li}^7$ . *Phys. Rev.* **108**, 1025–1027 (1957)
63. C.W. Li, R. Sherr, Inelastic scattering of alpha particles by lithium. *Phys. Rev.* **96**, 389–393 (1954)
64. H. Yamaguchi, T. Hashimoto, S. Hayakawa, D.N. Binh, D. Kahl, S. Kubono, Y. Wakabayashi, T. Kawabata, T. Teranishi,  $\alpha$  resonance structure in  $^{11}\text{B}$  studied via resonant scattering of  $^7\text{Li}+\alpha$ . *Phys. Rev. C* **83**, 034306 (2011)
65. H. Bohlen, N. Marquardt, W. Von Oertzen, P.H. Gorodetzky, Nucleon exchange in the low-energy scattering of  $\alpha$ -particles on  $^6\text{Li}$  and  $^7\text{Li}$ . *Nucl. Phys. A* **179**(2), 504–512 (1972)
66. J.P. Stoquert, N. Bendjaballah, H. Beaumevieille, C. Gérardin, R. Seltz, Niveaux excités de  $^{11}\text{B}$  observés dans la diffusion  $^4\text{He} + ^7\text{Li}$ . *J. Phys. France* **40**(9), 813–817 (1979)
67. G. Manning, B. Singh, A note on the  $^{10}\text{B}(\alpha, p)^{13}\text{C}$  reaction. *Proc. Phys. Soc. Sect. A* **66**(9), 842–843 (1953)
68. L. Van der Zwan, K.W. Geiger, The  $^{10}\text{B}(\alpha, n)^{13}\text{N}$  cross section for  $\alpha$ -energies from 1.0–5 MeV. *Nucl. Phys. A* **216**(1), 188–198 (1973)
69. H. Chen, X.M. Wang, L. Shao, J.R. Liu, A.C. Yen, Wei kan Chu., Cross-sections of  $^{10}\text{B}(\alpha, p)^{13}\text{C}$  nuclear reaction for boron analysis. *Nucl. Instruments Methods Phys. Res. Sect. B* **211**(1), 1–6 (2003)
70. L.C. McIntyre, J.A. Leavitt, M.D. Ashbaugh, Z. Lin, J.O. Stoner, Cross sections for  $170.5^\circ$  backscattering of  $^4\text{He}$  by the isotopes of boron for  $^4\text{He}$  energies between 1.0 and 3.3 MeV. *Nucl. Instruments Methods Phys. Res. Sect. B* **64**(1), 457–460 (1992)
71. Georgeanne R. Caughlan, William A. Fowler, Thermonuclear reaction rates v. Atomic Data Nucl Data Tables **40**(2), 283–334 (1988)
72. E.T. Jurney, J.W. Starner, J.E. Lynn, S. Raman, Thermal-neutron capture by  $^{14}\text{N}$ . *Phys. Rev. C* **56**, 118–134 (1997)
73. G. M. Hale, P. G. Young, M. Chadwick, and Z.-P. Chen. New Evaluations of Neutron Cross Sections for  $^{14}\text{N}$  and  $^{16}\text{O}$ . In Syed M. Qaim, editor, Nuclear Data for Science and Technology, pages 921–923, Berlin, Heidelberg, 1992. Springer Berlin Heidelberg
74. H. Fletcher Gabbard, Bichsel, and T.W. Bonner, The disintegration of nitrogen by fast neutrons. *Nucl. Phys.* **14**(2), 277–294 (1959)
75. J.H. Gibbons, R.L. Macklin, Total neutron yields from light elements under proton and alpha bombardment. *Phys. Rev.* **114**, 571–580 (1959)
76. C.H. Johnson, H.H. Barschall, Interaction of fast neutrons with nitrogen. *Phys. Rev.* **80**, 818–823 (1950)
77. G.L. Morgan, Cross sections for the  $^{14}\text{N}(n, p_0)$ ,  $(n, \alpha_0)$ , and the  $(n, \alpha_1)$  reactions from 0.5 to 15 MeV. *Nucl. Sci. Eng.* **70**, 163–176 (1979)
78. M. Niecke, M. Niemeier, R. Weigel, H. Wirzba-Lorenz, Angular distributions of neutron polarization from the  $^{14}\text{C}(p, n)^{14}\text{N}$  and  $^{11}\text{B}(\alpha, n)^{14}\text{N}$  reactions and  $R$ -matrix analysis of  $^{15}\text{N}$  in the excitation-energy range between 11.5 and 12.5 MeV. *Nucl. Phys. A* **289**(2), 408–424 (1977)
79. F.C. Young, A.S. Figuera, C.E. Steerman, Properties of the 12.50 and 12.52 MeV levels of  $^{15}\text{N}$ . *Nucl. Phys. A* **173**(2), 239–247 (1971)
80. W.D. Roseborough, J.J.G. McCue, W.M. Preston, C. Goodman, The Reaction  $\text{C}^{14}(p, n)\text{N}^{14}$ : Excited States in  $\text{N}^{15}$ . *Phys. Rev.* **83**, 1133–1136 (1951)
81. Richard M. Sanders, Study of the  $\text{C}^{14}(p, n)\text{N}^{14}$  and  $\text{C}^{14}(\alpha, n)\text{O}^{17}$  Reactions. *Phys. Rev.* **104**, 1434–1440 (1956)
82. W.R. Harris, J.C. Armstrong, Elastic scattering of 1- to 2.7-MeV Protons by  $\text{C}^{14}$ . *Phys. Rev.* **171**, 1230–1241 (1968)
83. Jerry D. Henderson, Emmett L. Hudspeth, William R. Smith, Capture and elastic scattering of protons by  $^{14}\text{C}$ . *Phys. Rev.* **172**, 1058–1062 (1968)
84. R.A. Dayras, Z.E. Switkowski, T.A. Tombrello,  $^{14}\text{C}$  production by the reaction  $^{11}\text{B}(\alpha, p)^{14}\text{C}$ . *Nucl. Phys. A* **261**(3), 365–372 (1976)
85. A. Turowiecki, A. Saganek, M. Siemiński, E. Wesołowski, Z. Wilhelmi, The  $^{11}\text{B}(\alpha, p)^{14}\text{C}$  reaction below 1.7 MeV bombarding energy. *Nucl. Phys. A* **468**(1), 29–37 (1987)
86. R.J. deBoer, C.R. Brune, M. Febraro, J. Görres, I.J. Thompson, M. Wiescher, Sensitivity of the  $^{13}\text{C}(\alpha, n)^{16}\text{O}$ s factor to the uncertainty in the level parameters of the near-threshold state. *Phys. Rev. C* **101**, 045802 (2020)

87. M. Pignatari, F. Herwig, R. Hirschi, M. Bennett, G. Rockefeller, C. Fryer, F.X. Timmes, C. Ritter, A. Heger, S. Jones, U. Battino, A. Dotter, R. Trappitsch, S. Diehl, U. Frischknecht, A. Hungerford, G. Magkotsios, C. Travaglio, P. Young, NuGrid Stellar Data Set. I. stellar yields from H to Bi for stars with metallicities  $Z = 0.02$  and  $Z = 0.01$ . *Astrophys. J. Suppl. Ser.* **225**, 24 (2016)
88. R.H. Cyburt, A.M. Amthor, R. Ferguson, Z. Meisel, K. Smith, S. Warren, A. Heger, R.D. Hoffman, T. Rauscher, A. Sakharuk, H. Schatz, F.K. Thielemann, M. Wiescher, The JINA REACLIB database: its recent updates and impact on type-I X-ray bursts. *Astrophys. J. Suppl. Ser.* **189**, 240–252 (2010)